PERINATAL JOURNAL

Original Article

Perinatal Journal 2025; 33(1):449-466

https://doi.org/10.57239/prn.25.03310051

Flow characteristics of a converging nozzle flow with sudden expansion at sonic Mach number

Newaz Md Ashif[1], Syed Ahmed Imran Bellary[2], Vinayak Hanmantasa Khatawate[3], Shamitha Shetty[4], Sher Afghan Khan[5]*

[1]Department of Mechanical and Aerospace Engineering, Faculty of Engineering, International Islamic University, Kuala Lumpur, 53100, Malaysia 2.
[2]Department of Robotics and Automation, Zeal College of Engineering and Research, Narhe, SPPU Pune-411041, Maharashtra, India
[3]Department of Mechanical Engineering, SVKM's Dwarkadas J. Sanghvi College of Engineering, Mumbai, India,
[4]Department of Mathematics, Nitte Meenakshi Institute of Technology, Nitte (Deemed to be University), Bangalore 560064, Karnataka, India
[5]Department of Mechanical and Aerospace Engineering, Faculty of Engineering, International Islamic University, Kuala Lumpur, 53100, Malaysia

Abstract

The development of space shuttles and high-performance military aircraft has made studying turbulent flow in a separated region a vital topic of study. Researchers are also interested in turbulent flow in transonic and supersonic flow. There is considerable relief for the flow when it separates and expands once the area of the larger duct suddenly increases. There are two areas where the shear layer emerges: the separated flow and the main flow. Considerable drag results from the split streamline reattaching to the duct, creating a recirculation zone where the pressure is lower than the surrounding air. Flow from a converging nozzle is suddenly exhausted to a larger diameter. The duct diameter is 22 mm. Base pressure management using a D-shaped rib as a passive control mechanism is the primary focus of this study. The passive control was located at various positions, with a length-to-diameter ratio (L/D) of 0.5, 1, 1.5, 2, and 3. Numerical simulations were conducted for 0.5, 1, and 1.5 mm rib radii. Results indicated that the D-shape rib with a 0.5 mm radius is ineffective, except at nozzle pressure ratios of 4 and 5. The maximum increase in the base pressure is attained for a rib radius of 1.5 mm, and a very moderate rise is obtained for a 1 mm radius. It is observed that the rib locations at L/D = 2 and 3 are ineffective, as the flow becomes attached to the wall around L/D = 1 to 1.5. Hence, one can select the rib radius and height based on the user's requirements.

Keywords: Base pressure, L/D ratio, Nozzle pressure Ratio, Sonic Mach number, Base drag

Introduction

Since the inception of fluid science, turbulence has remained a mystery. Turbulence is a part of the natural and artificial flows around us, and we need to comprehend it. To manage the drag associated with turbulent flows, it is essential to understand turbulence. Turbulence is sought in some flows when fluids are combined or when an increase in skin friction drag is needed. However, turbidity is undesirable in engineering flows and should be managed to reduce energy input. In engineering and real-world processes, turbulent drag is associated with significant ecological and financial repercussions. Fossil fuels are applied through a variety of methods. Since the inception of fluid science, turbulence has remained a mystery. Turbulence is a part of the natural and artificial flows around us, and we need to comprehend it. To manage the drag associated with turbulent flows, one must understand turbulence. Turbulence is sought in some flows when fluids are combined or when an increase in skin friction drag is needed. Turbulence is undesirable in engineering flows and should be managed to reduce energy input. In engineering and real-world processes, turbulent drag is associated with significant ecological and financial repercussions. Fossil fuels are applied through a variety of procedures.

The flow fields with sudden expansion are utilized in various fascinating and valuable applications, including parallel diffusers, propulsion systems, and combustion chambers. These flows have been studied because of the necessity of managing such flow fields. Because they produce the desired outcome without requiring additional mechanisms, as active control does, passive control mechanisms have long drawn the attention of scientists due to their simplicity and ease of use. However, the passive control remains with the system as a liability, and this dead weight remains with the system, unlike launch vehicles, which we discard once the propellant is wholly burned. One of the most significant advantages of dynamic control is that it can be utilized as needed.

Correspondence: Sher Afghan Khan, Department of Mechanical and Aerospace Engineering, Faculty of Engineering, International Islamic University, Kuala Lumpur, 53100, Malaysia **e-mail:** sakhan@iium.edu.my, **Received:** July 3, 2025 **Accepted:** September 1, 2025

Numerous applications, including high-speed aircraft, jet engines, rocket motors, rapid entry into a planetary atmosphere, gas pipelines, and commercial uses such as abrasive blasting, utilize the compressible flow effect. While incompressible flow primarily deals with constant density, compressible flow encompasses a variable range of density flows, from subsonic to supersonic.

The analysis of turbulent flow remains an area of ongoing research, driven partly by the development of high-speed missiles, unguided rockets, and supersonic military aircraft.

Flow separation, recirculation, and reattachment are complex characteristics of the axisymmetric expansion flow field. The two primary regions where a shear layer may separate in such a flow field are the recirculation flow region and the primary flow region. The point at which the separating streamline hits the wall is known as the reattachment line. A lot of information regarding sudden expansion issues can be found in the literature. They are, nevertheless, applicable to specific flow and geometrical parameter scenarios. Lowering turbulent drag will help mitigate global warming by reducing CO_2 emissions from the burning of fossil fuels. As a result, efforts should be made to eliminate the near-wall organized structures that significantly contribute to drag production. These near-wall structures can be modified using passive or active control techniques. It is simple to use passive methods, such as splitter plates, riblets, Gurney flaps, bleed, and super-hydrophobic surfaces; however, the drag reduction is relatively small. Active control approaches, on the other hand, can significantly reduce skin friction. Although active control methods can be challenging to implement and require feedback loops, the rewards of exploring different innovative active control methods are alluring.

2. Literature Review

The flow field at sonic and supersonic Mach numbers presents complex challenges due to flow separation, recirculation zones, and base pressure deficits, contributing significantly to aerodynamic drag. Researchers have extensively explored passive control methods, such as incorporating ribs, cavities, and other geometric modifications, to mitigate these issues and enhance base pressure recovery. Khan et al. [1] conducted experimental investigations using semi-circular ribs in suddenly expanded flows at both sonic and supersonic Mach numbers. Their study compared experimental results with predictions from single-layer and deep neural network models, demonstrating that including ribs effectively increased base pressure and reduced flow separation.

In a complementary study, Khan, Mazlan, and Sulaeman [2,27] examined the effect of ribs as passive control devices on base pressure at sonic Mach numbers. Their findings indicated that the presence of ribs led to a significant increase in base pressure, attributed to the disruption of the recirculation zone and the promotion of earlier flow reattachment. Further exploring rib geometries, Khan et al. [3] analyzed the impact of various rib configurations in a suddenly expanded flow at sonic Mach numbers. The study revealed that specific rib shapes and placements could optimize base pressure recovery, highlighting the importance of geometric considerations in passive control strategies. Numerical simulations have also played a pivotal role in understanding flow behaviors. Khan, Mazlan, and Ismail [4] performed simulations of suddenly expanded flows from converging nozzles at sonic Mach numbers, providing insights into velocity distributions and base pressure variations. Their work highlighted the importance of nozzle geometry and expansion ratios in shaping flow characteristics.

Advancements in computational fluid dynamics (CFD) have facilitated more comprehensive analyses. Khan et al. [5,28] conducted a CFD study on base pressure control using quarter ribs in sudden expansion ducts at sonic Mach numbers. The research demonstrated that quarter ribs could effectively manipulate the flow field, enhancing base pressure and reducing drag. Building upon this, Khan et al. [6] explored using semi-circular ribs at critical Mach numbers. Their findings emphasized the effectiveness of these ribs in controlling base pressure, particularly at specific Mach number regimes. A considerable amount of data is available in the literature regarding abruptly expanded flow issues, as discussed by Gao & Liu [7], Li et al. [8], Lu et al. [9], and Yan et al. [10], which outline the procedures governing base flows. Passive controls often involve geometric adjustments to the expanded duct, such as cavities and ribs, and modify the jet control to alter the shear layer's stability characteristics and function as flow control. Passive controls are typically less expensive and easier to build. Cavities, such as base and ventilated cavities, are among the most commonly used flow control technologies for regulating flow in abruptly increased flows, and they can enhance base pressure according to the system's needs. Pandey and Rathakrishnan [3] investigated the flow through an axisymmetric duct with annular cavities spaced at regular intervals. They discovered that adding cavity circulation reduces the oscillatory nature of the flow in the enlarged duct, allowing it to increase smoothly from the low pressure to the ambient pressure at which the jet was discharged. Rathakrishnan et al. [11] expanded the analysis to include multiple aspect ratios. They reported that the cavity in the expanded duct had a considerable impact, with the effect being more substantial for longer ducts than shorter ones.

Pandey and Rathakrishnan [12] conducted similar studies for highly subsonic to supersonic flows. They discovered a supplementary circulation to prevent the flow from oscillating due to cavities. This influence was more noticeable in subsonic than supersonic flow regimes. They also found that the enlarged conduit area ratio has a significant effect on base pressure and flow development. Pathan et al. [13] also produced a similar observation. Vikramaditya et al. [14] conducted an experimental study to investigate the impact of the base cavity on pressure changes in the base section of a conventional missile system with a high Mach number of 0.7. The primary objective of the investigation was to identify pressure changes and the main factors that drive them. Because the flow is substantially non-uniform, they discovered that the base pressure variation features varied significantly throughout the azimuthal direction due to model asymmetry. They also found that the introduction of the base cavity results in a long-term improvement in base pressure. Khan et al. [15] investigated the benefits of employing multiple cavities to minimize base drag in compressible subsonic flow. By minimizing base drag, the innumerable holes can regulate the base pressure. They concluded that the longer the duct, the more efficient the control using many cavities. Numerous cavities affect the wall pressure at lower L/D ratios but not at higher L/D ratios.

Similarly, the geometric dimensions of the cavity itself determine the base pressure. Khan et al. [15,29] also further investigated the effectiveness of the dimple in controlling the base pressure at subsonic expanded flow. The base drag will decrease with an increase in base pressure. At lower L/D, the wall pressure is affected; however, at higher L/D, it is not. In this case, the base pressure is also influenced by the geometric parameters of the cavities. Furthermore, Asadullah et al. [16] investigate the effect of single and multiple holes on base fluxes. They concluded that many cavities had a substantially more significant impact on base flows than single cavities.

Rajendran et al. [17] investigated suddenly expanded duct flows with significantly larger cross-sectional areas. They discovered that when NPR increases, the difference in base pressure reduces progressively. The wall pressure of a constant NPR changes continuously over the length of the duct and reaches ambient pressure when the flow passes the duct outlet. Finally, they concluded that the cavity aspect ratio had a significant influence on the flow field and base pressure. They also developed a low-cost, multi-channel data acquisition system (DAQ) and compared it to commercial DAQ systems. Recent research by Afzal et al. [18] and Afzal et al. [19] on supersonic Mach numbers is based on active control, backed by response surface analysis, k-means clustering, and data backpropagation modeling. The number of input variables for the data analysis was the same for the no-control and control groups. Bashir et al. [20] conducted a numerical investigation of turbulence models emphasizing turbulent intensity at low Reynolds number flows. Their work contributed to the selection of appropriate turbulence models for accurate flow simulations.

Baig et al. [21] explored the control of base flows with micro jets, demonstrating the effectiveness of active control methods in managing base pressure and reducing drag. Rehman and Khan [22] focused on controlling base pressure with micro-jets, providing insights into the design and implementation of active flow control techniques.

Faheem et al. [23] conducted an experimental study on the mean flow characteristics of a supersonic multiple-jet configuration, contributing to an understanding of complex jet interactions in high-speed flows. Sajali et al. [24] performed a numerical investigation of the flow field of a non-circular cylinder, providing data relevant to flow control around bluff bodies. Khan et al. [25] investigated the passive control of base drag in compressible subsonic flow using multiple cavities, emphasizing the effectiveness of cavity configurations in reducing drag.

The following section outlines the methodological aspects related to the computational fluid dynamics of the proposed work.

3. Computational fluid dynamics

3.1 Governing equations

The following hypotheses are taken into consideration:

Turbulent flow is considered because of the turbulent viscous dissipation effects.

The fluid's viscosity varies with temperature and is compressible.

At atmospheric pressure, the flow exits the duct.

While scanning the literature, we found that the internal flow k-ε turbulence model is the most suitable, as it yields reasonably good results. Sutherland's three-coefficient viscosity model is expressed as follows:

$$\mu' = \mu'_o \left(\frac{T_a}{T_{a,o}}\right)^{3/2} \frac{T_{a,o}+S\prime}{T_a+S\prime} \quad (1)$$

The reference viscosity value in kg/m-s is denoted as μ'_o, where μ' represents the viscosity. T_a denotes static temperature; K represents the temperature of a standard reference, and S' is the temperature-dependent Sutherland constant. Three-dimensional continuity equation for compressible flow:

The equation for mass balance is as follows:

$$\frac{\partial \rho}{\partial t} + \underline{\nabla} \cdot (\rho \underline{V}) = 0 \quad (2)$$

Where the fluid's velocity is denoted by V. The equation for momentum balance is:

$$\frac{\partial}{\partial t}(\rho \underline{V}) + \underline{\nabla} \cdot (\rho \underline{V}\underline{V}) + \underline{\nabla} p = \underline{\nabla} \cdot \left[2\mu(\underline{\nabla}\underline{V})_o^S\right] + \underline{\nabla} \cdot (\tau_{=Re}) \quad (3)$$

Where $(\underline{\nabla}\underline{V})_o^S = (\underline{\nabla}\underline{V})^S - \frac{1}{3}(\underline{\nabla} \cdot \underline{V})\underline{I}$, $(\underline{\nabla}\underline{V})^S = \frac{\underline{\nabla}\underline{V}+\underline{\nabla}\underline{V}^T}{2}$ and $\tau_{=Re}$ is the turbulent stress tensor. The formulae for total energy are as follows:

$$\frac{\partial}{\partial t}\left[\rho\left(\frac{1}{2}V^2 + u_{int}\right)\right] + \underline{\nabla}\left[\rho\left(\frac{1}{2}V^2 + u_{int}\right)\underline{V}\right] = \underline{\nabla}\left(\lambda \underline{\nabla} T - p\underline{V} + 2\mu \underline{V} \cdot (\underline{\nabla}\underline{V})_o^S + \underline{V} \cdot \tau_{=Re}\right) \quad (4)$$

Where u_{int} is the internal energy, and λ is the thermal conductivity. Many internal flow simulations use the k-epsilon turbulence model due to its affordability, resilience, and sufficient accuracy. The Ansys Fluent program incorporates the k-epsilon (ε) turbulence model used in this research. The K-equation allowed us to calculate the turbulent kinetic energy.

$$\frac{\partial}{\partial t}(\rho k) + \underline{\nabla} \cdot (\rho \underline{V} k) = \underline{\nabla} \cdot \left[(\mu + \frac{\mu_t}{\sigma_k})(\underline{\nabla} k)\right] - \rho\varepsilon + M_x \quad (5)$$

The turbulent kinetic energy dissipation rate is denoted by ε, the turbulent Prandtl number is σ-k, and the word Mx is the turbulence generation. Precisely, the dissipation (or (-equation)) is controlled by,

$$\frac{\partial(\rho\varepsilon)}{\partial t} = -\underline{\nabla} \cdot (\rho\varepsilon\vec{V}) + \underline{\nabla} \cdot \left[\left(\mu + \frac{\mu_T}{\sigma_\varepsilon}\right)\nabla\varepsilon\right] - C_1 f_1 \left(\frac{\varepsilon}{k}\right) M - C_2 f_2 \frac{\varepsilon^2}{k} \quad (6)$$

Where $\mu_t = \rho f_\mu C_\mu k^2/\varepsilon$ denotes turbulent viscosity, and the arbitrary constants are denoted as $\overline{C_\mu} = 0.09$, $\overline{C_1} = 1.44$, $\overline{C_2} = 1.92$, $\overline{f_\mu} = 1$, $\sigma_k = 1.0$ and $\sigma_\varepsilon = 1.3$.

4. Finite Volume Method

Geometry and modelling

The finite volume technique (FVM) was employed to delve further into this investigation. The CFD simulation utilized the ANSYS FLUENT 2024/R2 software to evaluate the fluid flow through the nozzle. We are examining the impact of the D-shape of the rib using a passive control method. The two orientations of the D-shape rib are shown in Figure 1.

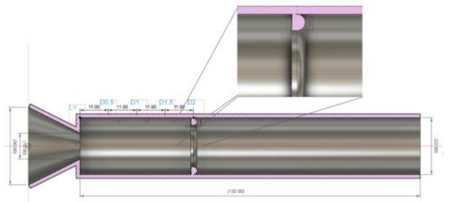

Fig. 1. Orientation of the ribeshing and boundary conditions

A crucial part of the CFD process is meshing. By choosing the free-face mesh type, the 2D model is of the structured mesh type in this case. Elements were assigned sizes according to the length of each line (edge) when the constructed structured mesh type was used. The lines were utilized to apply the element size, and elements with identical forms were created using face meshing. The mesh independence check is done. Figure 2 below shows the mesh's element type and size tested during the mesh independence check. Mesh independence test for duct 18 mm – without rib (L/D = 6). Different element sizes and their properties are based on the same geometry model.

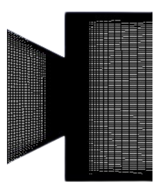

Close view

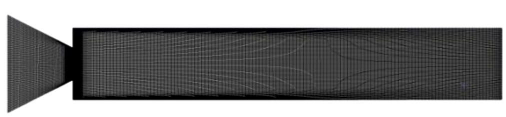

(a)Enlarged view

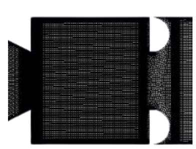

Enlarged view

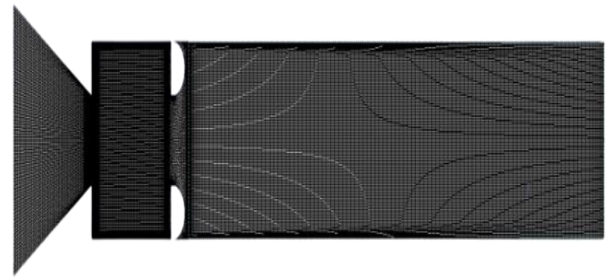

(b)

Fig. 2 Mesh model (a) without control, (b) with control

Assumptions and fluid properties

Assumptions are made to replicate the flow activities in the precise physical environment. Appropriate mathematical and numerical models are selected to simplify the governing equations.

To solve the governing equations simultaneously, numerical modeling requires selecting the appropriate mathematical models, including the governing equations, boundary conditions, mesh quality, and numerical method. Despite its limitations in accurately representing physical phenomena, the computational method has been trusted for decades and offers sufficient insight into flow behavior. As a result, this calls for careful consideration of elements that closely resemble the flow behavior. This study pinpoints the presumptions that jeopardize the precise physical state. The following are the assumptions and characteristics covered in this study:

The flow is assumed to be a steady 2D flow because the geometry is symmetric. Hence, the assumption that the flow is 2-D is justified.

The density of the air is variable as the flow is compressible. The inlet pressure is the gauge pressure at that Mach number and NPR, and at the outlet of the duct, the gauge pressure is zero.

Turbulent flow significantly impacts turbulent viscous dissipation at a given flow velocity, so it is considered.

The viscosity of the fluid is dependent on temperature.

At standard atmospheric pressure, the flows leave the duct. At normal ambient pressure, they do not.

Since the flow via the nozzle is considered turbulent, the compressible flow field is represented by the k-epsilon standard model. The subsequent equations most appropriately characterize the turbulent flow.

Validation of experimental model

The ANSYS Workbench program utilized fluid flow (Fluent) analytical techniques throughout the computational fluid dynamics (CFD) procedure. The model was generated via a Design Modeler. Figure 3 depicts a converging nozzle that abruptly widens into a duct with five ribs. Rathakrishnan [25] experimental setup, the dimensions of the convergent-divergent nozzle with a suddenly expanded duct are as stated below.

Table 1. The geometries of the validation model

Parameters	**Dimensions**
Nozzle inlet diameter	30 mm
Nozzle outlet diameter	10 mm
Duct diameter	22 mm
Duct length	Varies from 1D to 6D
Converging length	20 mm
Rib width	3 mm
Rib height	Varies from 1mm to 3mm

Figure 3 illustrates the base pressure ratio data from current and earlier studies [25]. The experimental values were denoted by dotted lines, while the simulation results obtained using ANSYS Fluent were represented by straight lines. The present numerical analysis exhibited a percentage discrepancy of less than 10% compared to the previous experimental study. Consequently, the current work met the criteria for acceptability. The curves exhibited a consistent pattern, with each point closely following the next. As a result, based on the table and graph described before, the validation of the current work was successful.

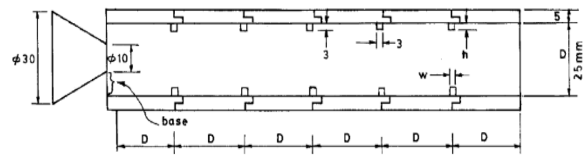

Fig. 3. Duct with five ribs used in an experimental study [26]

According to Rathakrishnan [26], the prior work was performed at aspect ratios of 3:3, 3:2, and 3:1; an area ratio of 6.25; L/D ranging from 1 to 6; pressure ratios of 1.141, 1.295, 1.550, 1.707, and 2.458; and nozzle exit Mach numbers of 0.44, 0.62, 0.82, 0.91, and 1.0. However, in a prior publication by Rathakrishnan [25]. The result, as shown in Figure 4, is the base pressure ratios with an L/D ratio at a fixed nozzle pressure ratio (P01/Pa = NPR) of 2.458, and models with control in the form of ribs with aspect ratios of 3:2 and 3:3 were chosen for comparison with the current CFD work. The simulation is supported by Rathakrishnan's [26] experimental work, which used five ribs positioned at equidistant intervals in the duct, as illustrated in Figure 4. The results of base pressure fluctuation with NPR of 2.458 and L/D ranging from 2 to 6 are obtained. The study is repeated to validate the numerical results of a model with control over different rib aspect ratios [26].

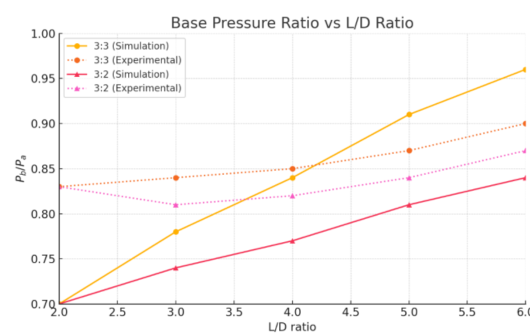

Fig. 4. Validation of previous work by Rathakrishnan [26]

Mesh independence study

Table 2 presents data from a mesh independence study, a crucial step in computational simulations that ensures the results remain consistent regardless of the mesh refinement level. The element sizes range from coarse to fine, with corresponding node and element counts for each mesh configuration. As the mesh becomes finer, the number of nodes and elements increases significantly, from 1,284 nodes and 1,145 elements in the coarsest mesh to 1,354,262 nodes and 1,351,303 elements in the finest mesh. This study aims to determine the optimal mesh size for accurate simulations without unnecessary computational expense. The table shows a notable increase in nodes and elements as the mesh is refined. The coarsest mesh has relatively few nodes and elements, resulting in a lower computational cost but potentially lower accuracy. Conversely, the finest mesh offers the highest resolution at the expense of significant computational resources. The medium and fine meshes provide intermediate levels of refinement, offering a balance between accuracy and efficiency.

Table 2. Mesh independence study

Element size	Coarsest	Coarse	Medium 1	Medium 2	Fine	Finer	Finest
Nodes	2703	5573	18053	35486	264734	762769	3885169
Elements	2500	5286	17577	34838	263101	760026	3879157

Based on the trends in node and element numbers, the finest mesh will likely produce the most accurate results (Figure 5). However, continuing to refine the mesh beyond a certain point may offer diminishing returns in terms of accuracy while significantly increasing computational time. A critical assessment of this table would suggest that the "Fine" or "Finer" mesh configurations may represent the best balance between accuracy and computational efficiency. These configurations substantially increase the number of nodes and elements compared to the medium meshes without reaching the computational expense of the finest mesh. If the simulation results do not change significantly between the fine and finest meshes, further refinement of the finest mesh is unnecessary, as it would only increase computational time without added benefit. Thus, the fine or finer mesh sizes are likely the best choices for further simulation.

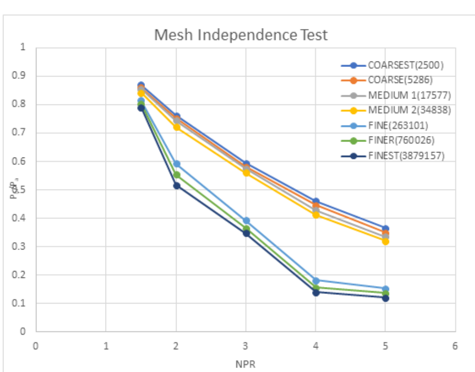

Fig. 5. Results of mesh check

5. Results and Discussions

Before examining the findings, it would be helpful to understand the mechanics underlying the sudden increase in relief to the flow. Figure 6(a) illustrates how the boundary layer at the nozzle exit would form a free shear layer for subsonic flows and meet the expanded duct wall downstream.

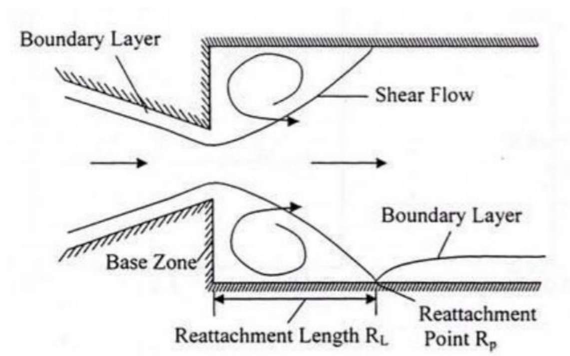

Fig. 6. (a) Sudden Expansion Flow Field

The reattachment point is the location where the flow attaches. Reattachment length is the distance between the base and the point of reattachment. One or more vortices will be positioned between the base, the reattachment point, and the edge of the free shear layer. The first, strong vortex near the base is referred to as the primary vortex. That moves fluid from the base to the main flow on the other side of the free shear layer edge. There is low pressure at the base due to this pumping motion. The pumping, however, also becomes periodic since vortex shedding is a periodic event. The base pressure varies as a result of this. Nonetheless, it was found that the base pressure variations were often minimal and could be expressed as a mean value. Oscillatory flow occurs throughout the duct due to the periodicity of the vortex motion. There are several flow and geometrical parameter combinations where the oscillations can get terrible. To adjust the primary vortex strength, the reattachment and the flow Mach number significantly impact the suction at the base and the flow oscillations in the duct.

Control and rib orientation

Figure 7 shows the orientation of the rib as 2. In this arrangement, the flat part of the rib faces the base region, and the curved part is downstream or at the aft of the rib. In the previous case, as shown in Fig. 6, the curved part of the rib faces the base region, and the vertically flat part is downstream. In this study, the ribs were kept at two different orientations to ascertain their effectiveness in both cases. As seen in Fig. 7, the shear layer, upon exiting the nozzle, allowed it to expand to a larger diameter of 22 mm, from the 10 mm converging nozzle exit diameter. In the following section, we will discuss the efficacy of the ribs for this orientation. In Fig. 7, this orientation is expected to result in better efficiency of the passive control.

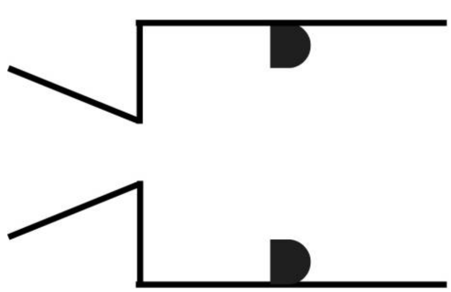

Fig. 7. Converging nozzle and duct assembly with d-shape rib and rib orientation

5.1 Base Pressure Results for Rib Location at L/D = 0.5

The findings of this study for orientation two are shown in Figs. 8 (a) to (f), where the flat surface of the rib will interact with the shear layer and is expected to increase the base pressure. Fig. 8(a) shows that the pattern of the base pressure is getting reversed for rib radii of 0.5 mm and 1 mm. The base pressure decreases for nozzle pressure ratios (NPR) of 1.5 to 2 for rib radii of 1 and 0.5, and for NPRs of 4 to 5. Similarly, there is an increasing trend for rib radii of 0.5 and 1mm for NPRs in the range of 1.5 to 3.5 and 2 to 5. This trend in the base pressure is not considered, as the rib is located at L/D = 0.5, and the flow is in transition and has not stabilized.

Similar trends in the base pressure are observed for other duct lengths, namely L/D = 5 to 6. There are marginal variations in the magnitude of the base pressure due to the influence of the ambient atmospheric pressure and the duct L/D ratio.

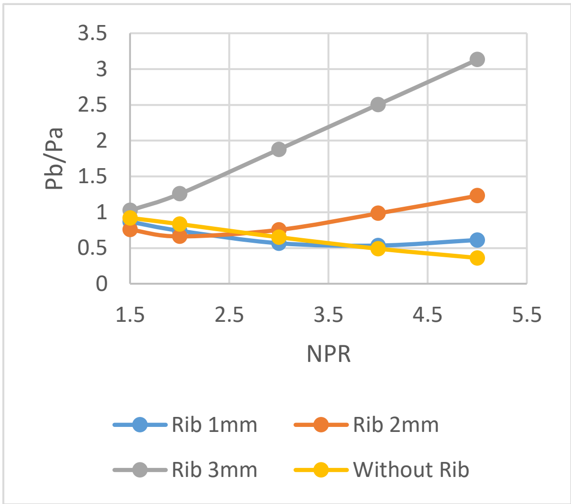

L/D = 1

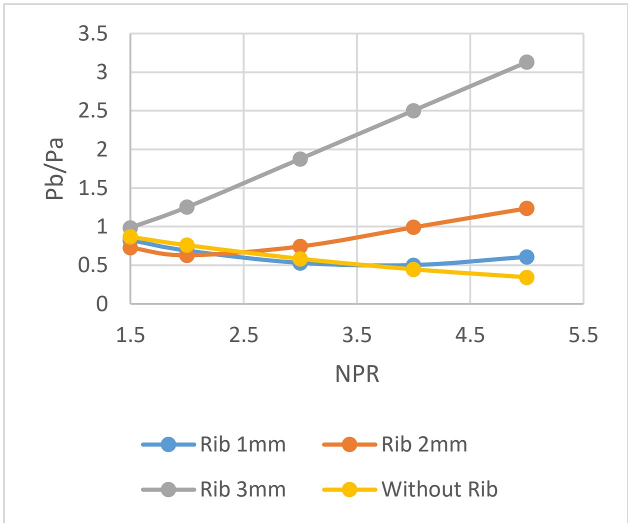

L/D = 2

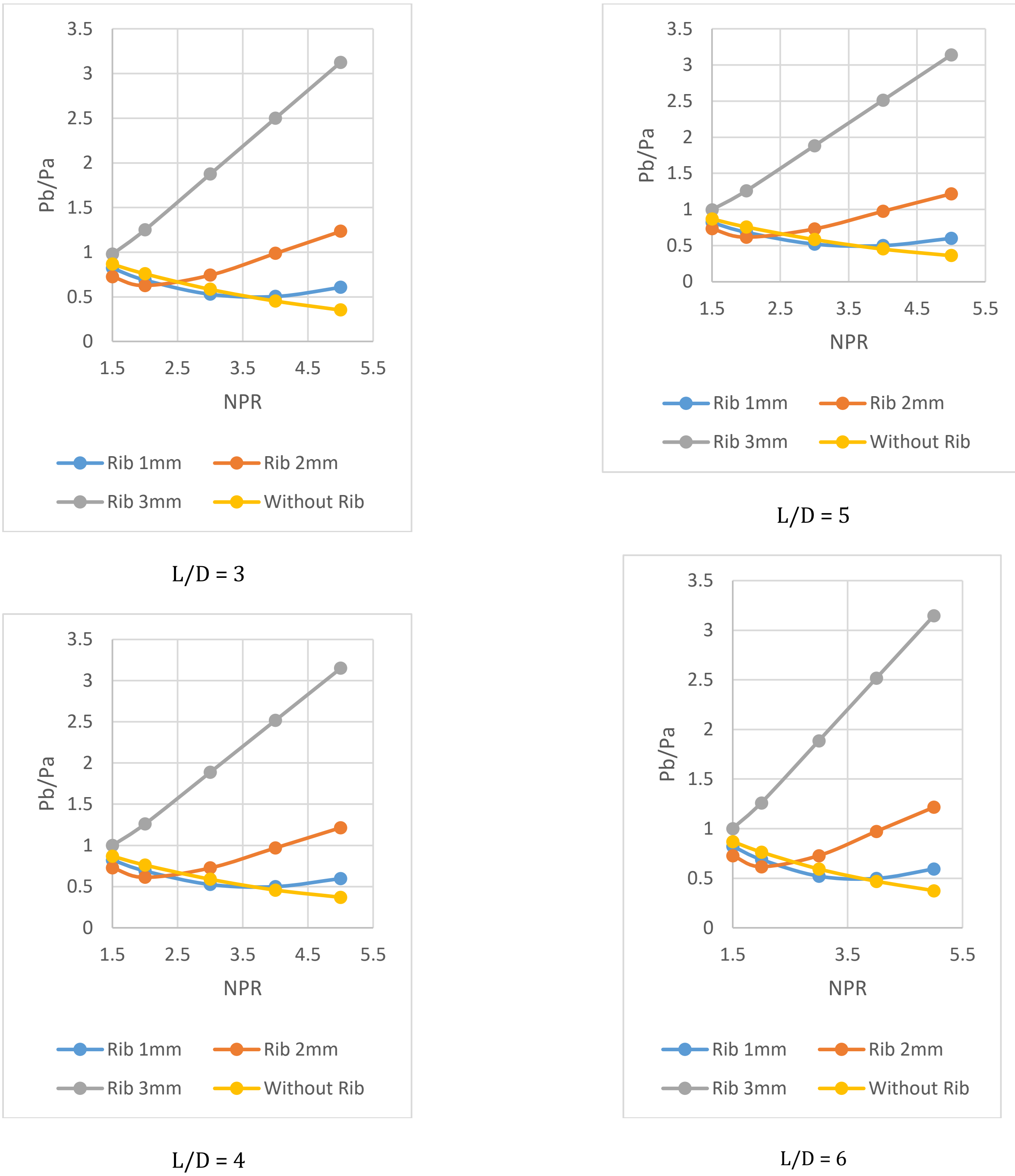

Fig. 8. Base pressure vs. npr for numerous duct segments

5.2 Base pressure results for rib location at l/d = 1.0

When the rib is located at L/D = 1, the findings of this study are shown in Figures 9 (a) to (e) for various NPRs and duct lengths. Fig. 9(a) presents the outcomes of the present study for a duct with L/D = 2. When we compare the base pressure results from the previous case, where the rib was placed at L/D = 0.5. As discussed earlier, when the rib is placed at L/D = 0.5, the separated flow is in transition and has not yet stabilized. Our apprehension is confirmed when we examine the base pressure results for the rib location at L/D = 1. The pattern of the results is remarkably different, as expected.

The figure shows that the control becomes effective for a rib radius of 0.5 mm, and the base increases nearly fifty percent compared to the case without ribs. In the case of rib radii of 1 mm and 1.5 mm, the declining trend is absent for the 1.5 mm rib, and for the 1mm rib, the decreasing trend is arrested once the flow is choked. However, the base pressure's magnitude is higher for a higher radius than the rib's lower radius.

Similar results are seen for other duct sizes, namely L/D = 3, 4, 5, and 6. For all these duct sizes, the base pressure values are nearly the same, with minor variations in the magnitude of the base pressure due to the influence of ambient atmospheric pressure.

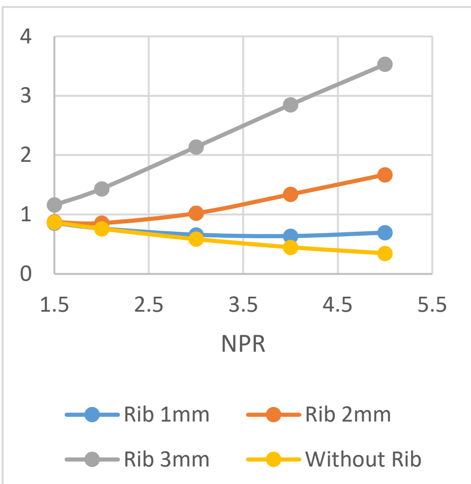

L/D = 2

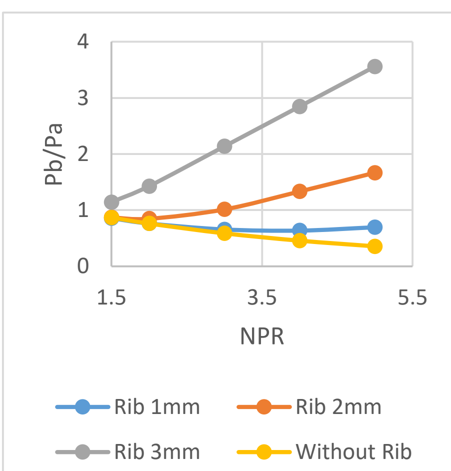

L/D = 3

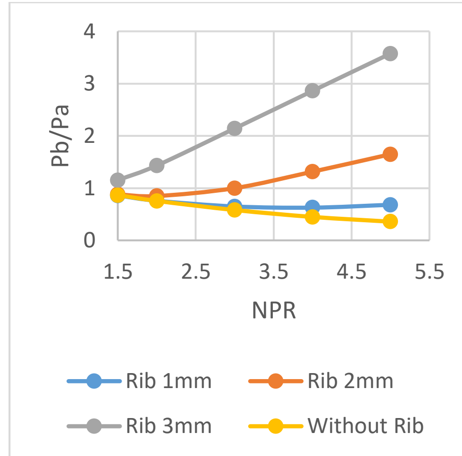

L/D = 4

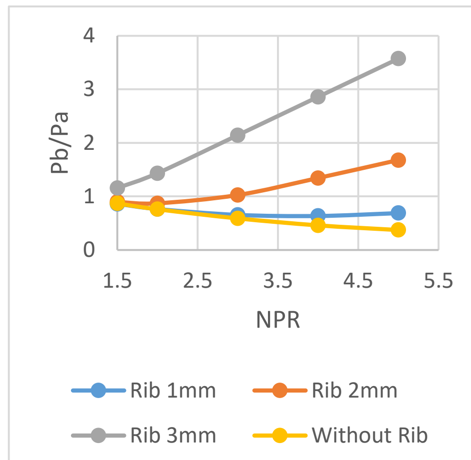

L/D = 5

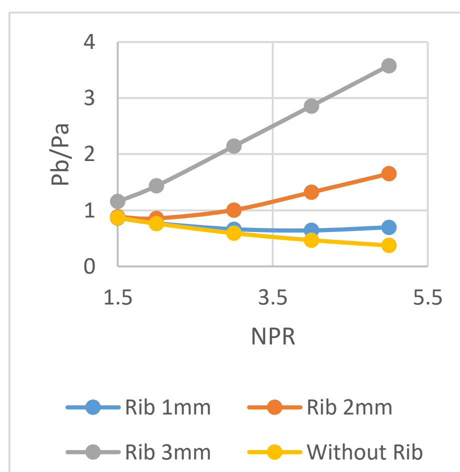

L/D = 6

Fig. 9. Base pressure vs. npr for numerous duct segments

5.3 *Base pressure results for rib location at l/d = 1.5*

When the rib is placed at L/D = 1.5, the study's outcomes are presented in Figures 10(a) to (e) for various duct sizes and levels of expansion. Figure 15(a) shows that a considerable change in the magnitude of the base pressure is found, which is more substantial for rib radii of 1 mm and 1.5 mm. There is a slight increase in the base pressure for a 0.5 mm rib radius.

These changes are attributed to the rib's location, which appears to be close to the reattachment point of the dividing streamline.

When we examine the base pressure results for other higher duct lengths, we find that their magnitude is almost the same, except for nominal changes in base pressure due to variations in duct sizes and the impact of ambient atmospheric pressure.

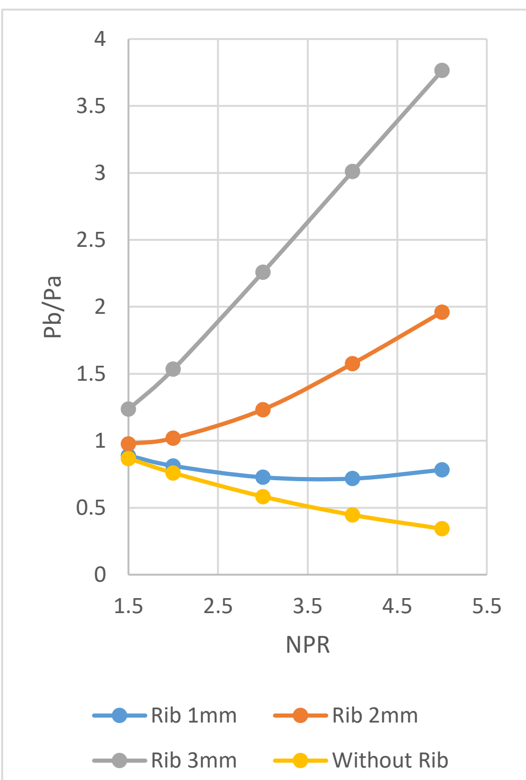

L/D = 2

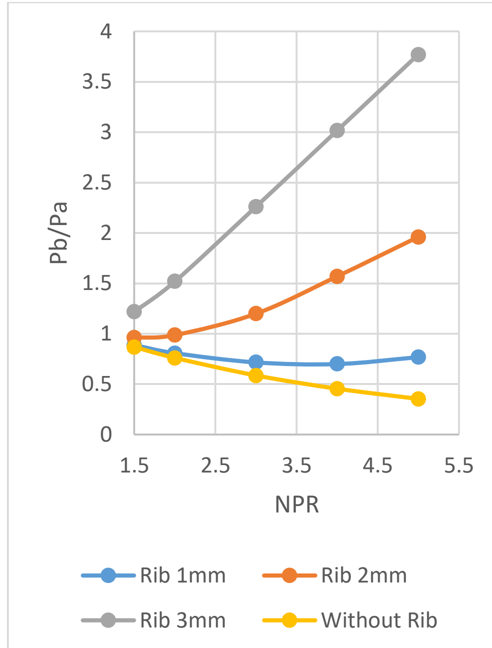

L/D = 3

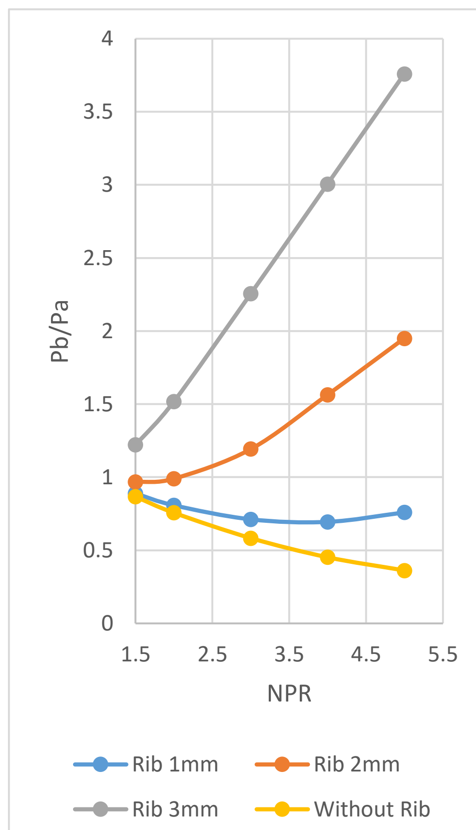

L/D = 4

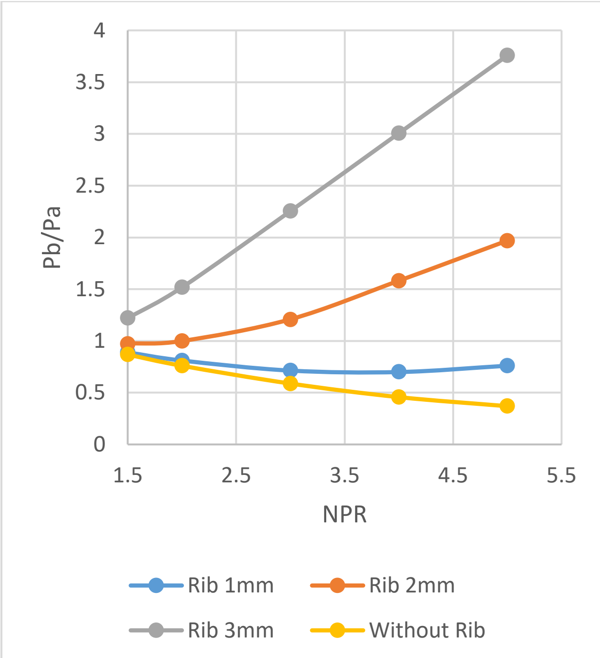

L/D = 5

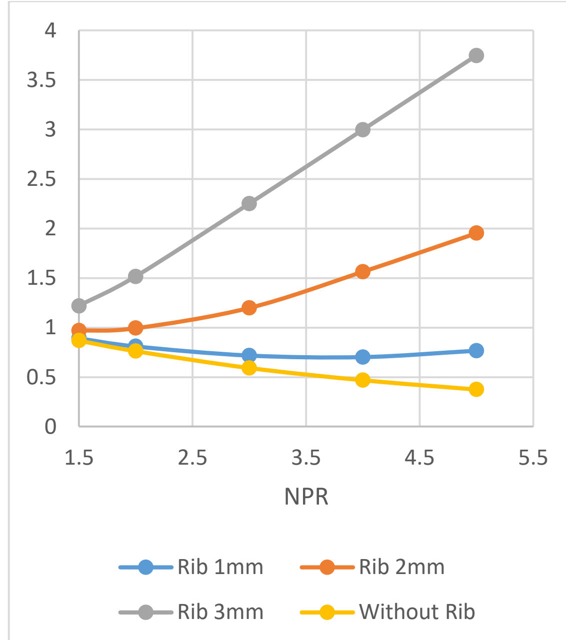

L/D = 6

Fig. 9. Base pressure vs. npr for numerous duct segments

5.4 Base pressure results for rib location at l/d = 2.0

When the rib is located at L/D = 2, the base pressure resulting from this study is illustrated in Figures 10(a) to (d) for various duct sizes and nozzle pressure ratios. As discussed earlier, for a duct diameter of 22 mm, the reattachment length appears to be approximately L/D = 1 to 1.5. Once the flow is attached to the wall and the passive control mechanism is also located within the reattachment point, further shifting the rib location downstream will not result in a considerable gain in base pressure. The base pressure results are to be analyzed, taking into account these factors.

As already mentioned, the base pressure values do not change much due to increased duct length from L/D = 3 to 6. Marginal changes, if any, are caused by the shock wave interactions with the duct wall, secondary vortices generated from the rib's sharp corner, and the impact of back pressure.

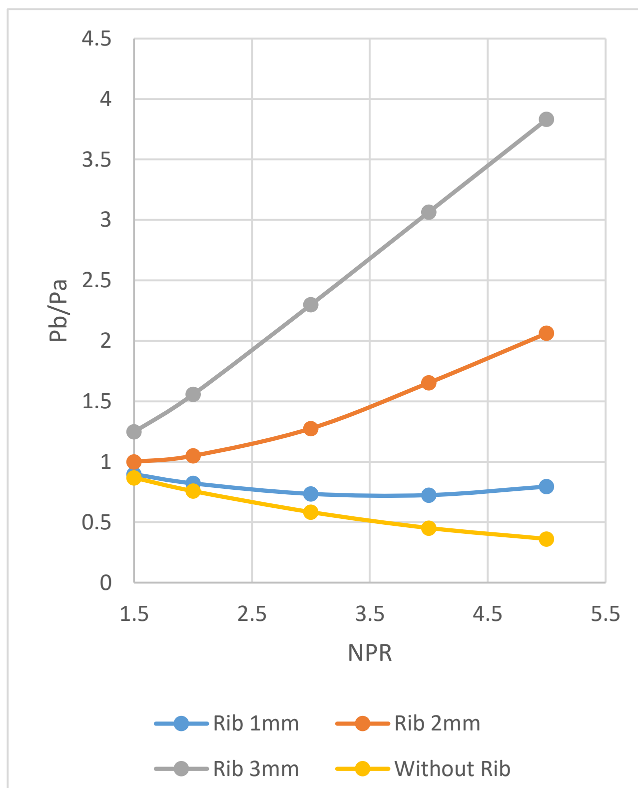

L/D = 3

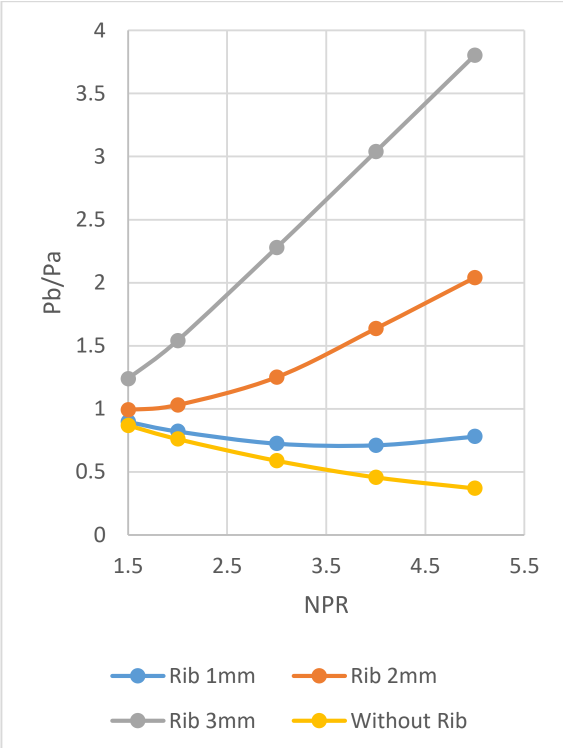

L/D = 4

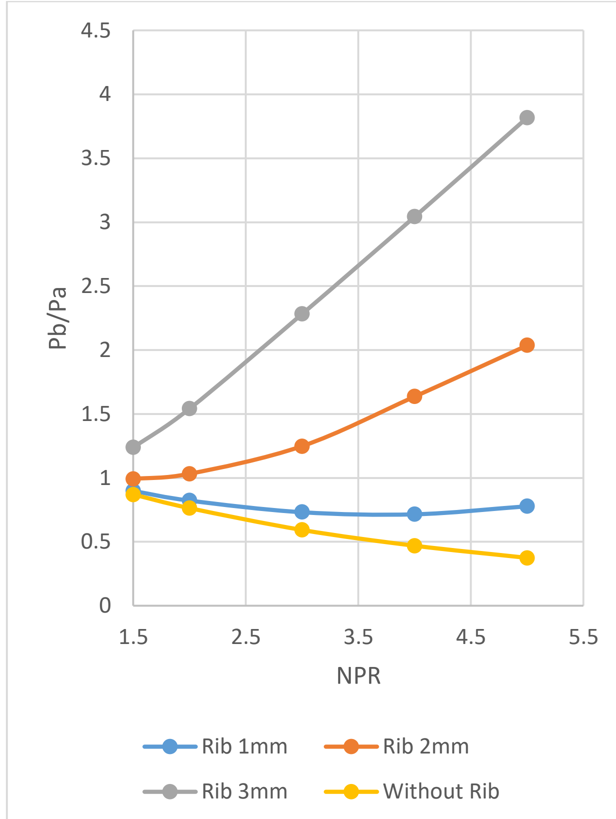

L/D = 6

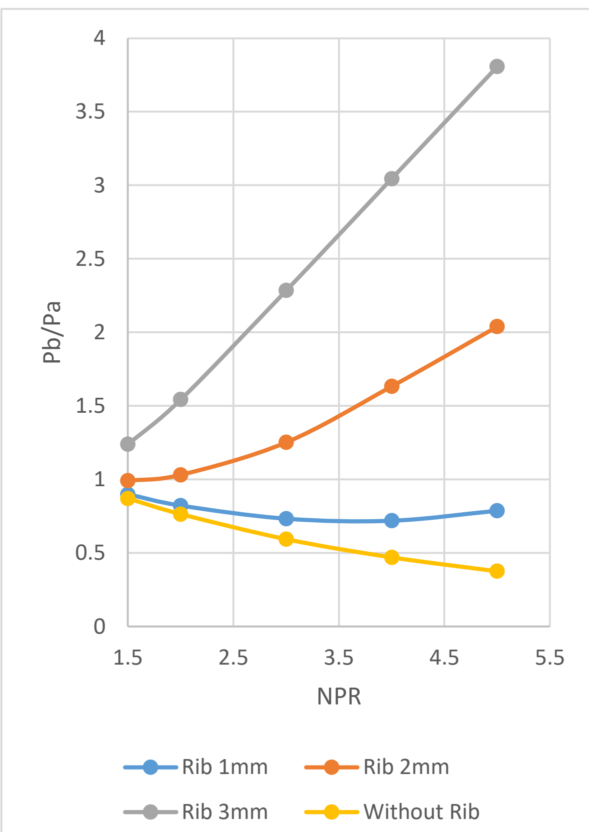

L/D = 5

Fig. 10. Base pressure vs. npr for numerous duct segments

5.5 Base pressure results for rib location at l/d = 3.0

Finally, the outcomes of this study are presented in Figures 11(a) to (c) for the same range of nozzle pressure ratios and duct sizes, specifically L/D = 4, 5, and 6. As mentioned earlier, once the flow is established and the passive control in the form of a D-shaped rib is placed at L/D = 3, it does not yield encouraging results; there is no reverse flow from the reattachment point, which is necessary for this case to enhance the base pressure. Even though there is a marginal increase in the base pressure, it is not worth mentioning as the gain achieved for the rib location at L/D = 1 and 1.5 remains almost unchanged, even though the rib has been relocated towards the downstream of the duct. The same is true for this location of the rib; as the duct sizes increase, there is not much change in the magnitude of the base pressure.

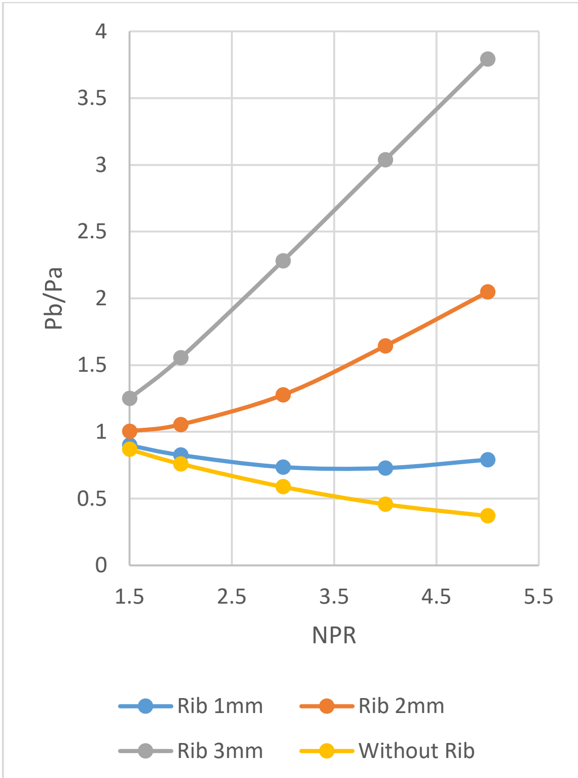

L/D = 4

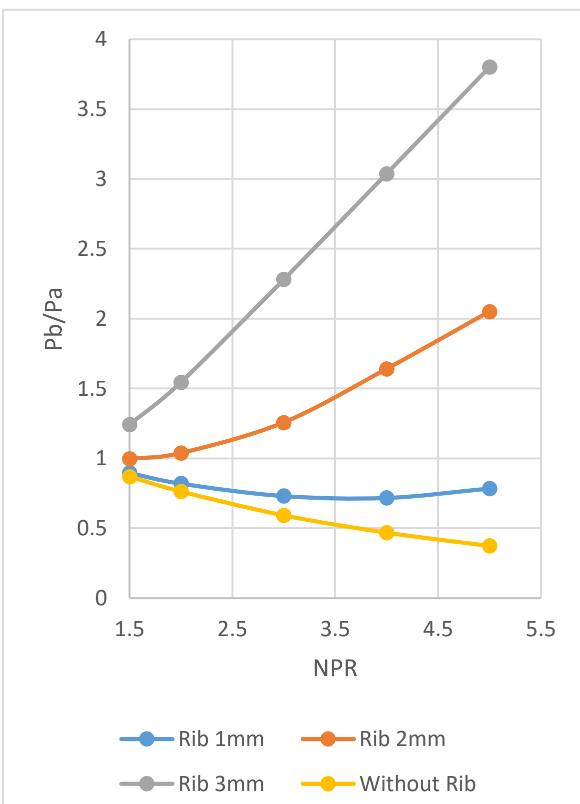

L/D = 5

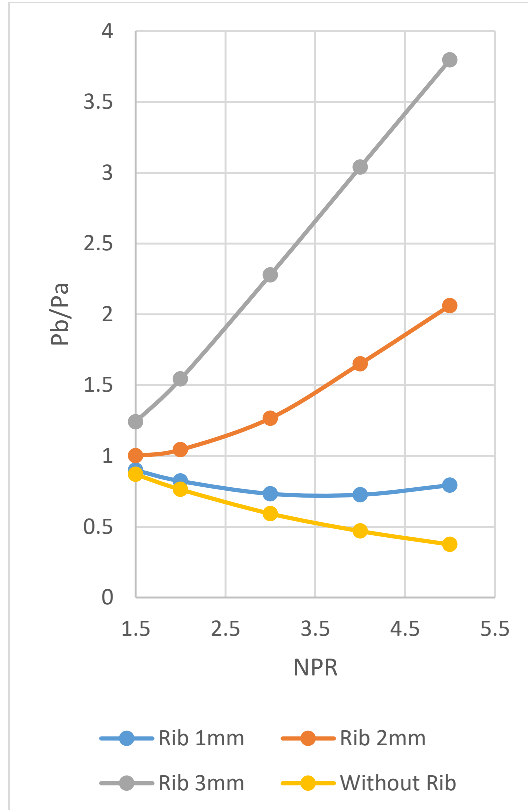

L/D = 6

Fig. 11. Base Pressure Vs. NPR for numerous Duct segments

6. Conclusions

Based on the discussion above, we may conclude that the base pressure is a strong function of the nozzle pressure ratio and the rib locations. In this study, we have considered two orientations of the rib. For orientation one, the curved part of the D-shaped rib faces the exiting shear layer from the converging nozzle, and in orientation two, the straight part of the rib faces the shear layer. The results show that the base pressure values are slightly higher for orientation two than for rib orientation. This change is due to the sharp corner being upstream and downstream for other orientations.

For this duct diameter, the reattachment length seems to be around L/D = 1 to 1.5. That may be the main reason that when the rib is shifted to L/D = 2 and 3, it does not substantially increase the base pressure. As we know, this increase in the base pressure is due to the interaction of the waves, the location of the reattachment point, duct size, and the strength of the secondary vortices.

For rib location L/D = 0.5, the flow is in transition and has not been established; hence, the base pressure values are lower than the base pressure values for rib locations at L/D = 1 and 1.5.

There is a progressive rise in the base pressure values when the rib is located at L/D = 1, and then when the rib is located at L/D = 1.5, there is a marginal change in the base pressure values. With a further shift in the rib locations downstream (i.e., L/D = 2 and 3), there is no change in the base pressure values, as they have reached a steady state. Hence, one suggestion is to analyze the results on a case-by-case basis. The reattachment length depends on the Mach number, duct diameter, expansion levels, and length-to-diameter ratio.

References

1 Khan, A., Rajendran, P., Sidhu, J.S.S., & Sharifpur, M. (2023). Experimental investigation of suddenly expanded flow at sonic and supersonic Mach numbers using semi-circular ribs: a comparative study between experimental, single-layer, deep neural network (SLNN and DNN) models. European Physical Journal Plus, 138(4), 314. https://doi.org/10.1140/epjp/s13360-023-03853-1

2 Khan, A., Mazlan, N.M., & Sulaeman, E. (2022). Effect of ribs as passive control on base pressure at sonic Mach numbers. CFD Letters, 14(1), 140–151. https://doi.org/10.37934/cfdl.14.1.140151

3 Khan, A., Khan, S.A., Raja, V., Aabid, A., & Baig, M. (2024). Effect of ribs in a suddenly expanded flow at sonic Mach number. Heliyon, 10(9), e30313. https://doi.org/10.1016/j.heliyon.2024.e30313

4 Khan, A., Mazlan, N.M., & Ismail, M.A. (2020). Numerical simulation of suddenly expanded flow from a converging nozzle at sonic Mach number. In Lecture Notes in Mechanical Engineering, pp. 349–359. https://doi.org/10.1007/978-981-15-4756-0_29

5 Khan, A., Akhtar, M.N., Aabid, A., Baig, M., & Khan, S.A. (2024). Comprehensive CFD analysis of base pressure control using quarter ribs in a sudden expansion duct at sonic Mach numbers. International Journal of Thermofluids, 24, 100908. https://doi.org/10.1016/j.ijft.2024.100908

6 Khan, A., Akhtar, M.N., Khan, S.A., Aabid, A., & Baig, M. (2024). Base pressure control with semi-circular ribs at the critical Mach number. Fluid Dynamics and Materials Processing, 20(9), 2007–2028. https://doi.org/10.32604/fdmp.2024.049368

7 Gao, S., & Liu, J. (2020). Adaptive neural network vibration control of a flexible aircraft wing system with input signal quantization. Aerospace Science and Technology, 96. https://doi.org/10.1016/j.ast.2019.105593

8 Li, S., Li, L., Huang, W., Zhao, Y., & Chen, J. (2020). Design and investigation of an equal cone-variable Mach number wave rider in hypersonic flow. Aerospace Science and Technology, 96. https://doi.org/10.1016/j.ast.2019.105540

9 Lu, J., Huang, J., & Lu, F. (2020). Kernel extreme learning machine with iterative picking scheme for failure diagnosis of a turbofan engine. Aerospace Science and Technology, 96. https://doi.org/10.1016/j.ast.2019.105539

10 Yan, C., Yin, Z., Shen, X., Mi, D., Guo, F., & Long, D. (2020). Surrogate-based optimization with improved support vector regression for non-circular vent hole on aero-engine turbine disk. Aerospace Science and Technology, 96. https://doi.org/10.1016/j.ast.2019.105332

11 Rathakrishnan, Ethirajan, Ramanaraju, O. V, & Padmanaban, K. (1989). Influence of Cavities on Suddenly Expanded Flow Field. Mechanics Research Communications, 16(3), 139-146.

12 Pandey, Krishna Murari, & Rathakrishnan, E. (2006). Influence of Cavities on Flow Development in Sudden Expansions. International Journal of Turbo and Jet Engines, 23(2), 97.

13 Pathan, K. A., Dabeer, P., & Khan, S. A. (2019). Effect of Nozzle Pressure Ratio and Control Jets Location on Control Base Pressure in Suddenly Expanded Flows. Journal of Applied Fluid Mechanics, 12(4), 1127-1135. https://doi.org/10.29252/jafm.12.04.29495

17 Vikramaditya, N., Viji, & Verma, S., & Ali, Naveed &

Thakur, D. (2017). Base Pressure Fluctuations on a Typical Missile Configuration in the Presence of Base Cavity. Journal of Spacecraft and Rockets. 55. 1-11. 10.2514/1.A33926.

18 Khan, S. A., Asadullah, M., Ahmaed, F.G.M., Jalaluddeen, A., Baig, & MAA. (2018). Passive Control of Base Drag in Compressible Subsonic Flow Using Multiple Cavity. International Journal of Mechanical and Production Engineering Research and Development, 8(4), 39-44. https://doi.org/10.24247/ijmperdaug20185

19 Asadullah, M., Khan, S. A., Soudagar, M. E. M., & Vaishak, T. R. (2018). A Comparison of the Effect of Single and Multiple Cavities on Base Flows. In 2018, IEEE 5th International Conference on Engineering Technologies and Applied Sciences (ICETAS) (pp. 1-5). IEEE.

20 Rajendran, P., Sethuraman, V., & Khan, S. A. (2019). A Cost-Effective Data Acquisition Instrumentation for Measurement of Base Pressure and Wall Pressure in Suddenly Expanded Flow-Through Ducts. Journal of Advanced Research in Fluid Mechanics and Thermal Sciences, 60(1), 112-123.

21Afzal, A., Aabid, A., Khan, A., Afghan, S., Rajak, U., Nath, T., & Kumar, R. (2020). Response surface analysis, clustering, and random forest regression of pressure in suddenly expanded high-speed aerodynamic flows. Aerospace Science and Technology, 107, 106318. https://doi.org/10.1016/j.ast.2020.106318

22 Afzal, A., Khan, S. A., Islam, T., Jilte, R. D., Khan, A., & Soudagar, M. E. M. (2020). Investigation and backpropagation modeling of base pressure at sonic and supersonic Mach numbers. Physics of Fluids, 32(July), 096109. https://doi.org/10.1063/5.0022015

23 Bashir, M., Rajendran, P., Khan, A., Raja, V., & Khan, S.A. (2023). Numerical investigation of turbulence models with emphasis on turbulent intensity at low Reynolds number flows. Advances in Aircraft and Spacecraft Science, 10(4), 303-315. https://doi.org/10.12989/aas.2023.10.4.303

24Baig, M.A.A., Khan, S.A., Al-Mufadi, F., & Rathakrishnan, E. (2011). Control of base flows with microjets. International Journal of Turbo and Jet Engines, 28(1), 59-69. DOI:10.1515/tjj 2011.009

14 Rehman, S., & Khan, S.A. (2008). Control of base pressure with micro-jets: Part I. Aircraft Engineering and Aerospace Technology, 80(2), 158-164. https://doi.org/10.1108/00022660810859373

15 Faheem, M., Afghan Khan, S., Asrar, W., Khan, A., & Kumar, R. (2021). Experimental study on the mean flow characteristics of a supersonic multiple jet configuration. Aerospace Science and Technology, 108, 106377. DOI:10.1016/j.ast.2020.106377

16 Sajali, M.F.M., Aabid, A., Khan, S.A., Sulaeman, E., & Mehaboobali, F.A.G. (2019). Numerical investigation of the flow field of a non-circular cylinder. CFD Letters, 11(5), 37-49. https://www.akademiabaru.com/submit/index.php/cfdl/article/view/3161

25 Khan, S.A., Asadullah, M., Fharukh Ahmed, G.M., Jalaluddeen, A., & Ali Baig, M.A. (2018). Passive control of base drag in compressible subsonic flow using multiple cavities. International Journal of Mechanical and Production Engineering Research and Development, 8(4), 39-44. DOI:10.24247/ijmperdaug20185

26 E Rathakrishnan. (2001). Effect of ribs on suddenly expanded flows. AIAA Journal 39(7), 1402-1404. https://doi.org/10.2514/2.1461.

27 Moghavvemi, S., Jam, F. A., & Iqbal Khan, T. (2025). The Impact of Motivation, Opportunity, Financial Ability, and Willingness on Resident Support for Tourism Development. Tourism Planning & Development, 22(1), 63-84.

28 Jam, F. A., Singh, S. K. G., Ng, B., & Aziz, N. (2018). The interactive effect of uncertainty avoidance cultural values and leadership styles on open service innovation: A look at malaysian healthcare sector. International Journal of Business and Administrative Studies, 4(5), 208-223.

29 Fathi, Ehsan, Mohammad Reza Ekhtesasi, Ali Talebi, and Jamal Mosaffaie. "Assessment of Ilam Dam Water Quality Using TLI, TSI, TSIM, and IRWQI Indices." Environment

and Water Engineering (2025).